

# Six New Galactic Orbits of Globular Clusters in a Milky-Way-Like Galaxy

Christine Allen<sup>1</sup>, Edmundo Moreno<sup>1</sup>, and Bárbara Pichardo<sup>1,2</sup>

## ABSTRACT

Absolute proper motions for six new globular clusters have recently been determined. This motivated us to obtain the Galactic orbits of these six clusters both in an axisymmetric Galactic potential and in a barred potential, such as the one of our Galaxy. Orbits are also obtained for a Galactic potential that includes spiral arms. The orbital characteristics are compared and discussed for these three cases. Tidal radii and destruction rates are also computed and discussed.

*Subject headings:* galaxy: halo — galaxy: kinematics and dynamics — globular clusters: general

## 1. INTRODUCTION

Absolute proper motions have become available for six new globular clusters (Casetti-Dinescu et al. 2007), thus increasing to 54 the number of globular clusters of our Galaxy for which full space velocities and Galactic orbits can now be calculated. In a previous paper (Allen, Moreno & Pichardo 2006, hereafter Paper I) Galactic orbits were computed for 48 globular clusters, using both an axisymmetric and a barred Milky-Way-like potential. We found that the effect of the bar was greatest for clusters with orbits residing mostly within the bar, and was negligible for the outermost clusters of our sample.

In the interim, Casetti-Dinescu et al. (2007) have obtained absolute proper motions for six additional clusters; they have also computed Galactic orbits in an axisymmetric potential. Since most of their cluster orbits appear to reside quite within the region of influence of the Galactic bar, it seems worthwhile to compute the orbits in a barred potential. Also, by computing orbits using different axisymmetric Galactic models some insight might be gained on the sensitivity of the results upon the potential model adopted.

---

<sup>1</sup>Instituto de Astronomía, Universidad Nacional Autónoma de México, México, D. F., México.

<sup>2</sup>Institute for Theoretical Physics, University of Zurich, Winterthurerstrasse 190, Zurich 8057, Switzerland.

In particular, Casetti-Dinescu et al. (2007) comment on the apparent “pairing” of the orbital parameters of NGC 2808 and NGC 4372, on one hand and NGC 4833, and NGC 5986 on the other. Since these “pairings” or kinematic groups may have important implications for the dynamical and merger history of our Galaxy (Kepley et al. 2007; Allen et al. 2007, and references therein), it is interesting to assess whether or not these similarities are sensitive to the Galactic model potential used.

In the present paper we compute Galactic orbits for the six new clusters, in the axisymmetric potential of Allen & Santillán (1991), in the barred model of Pichardo et al. (2004), as well as in a potential model including spiral arms (Pichardo et al. 2003).

As before, we find that the orbits in the barred potential generally do not show secular changes in the total energy,  $E$ , or in the  $z$ -component of the angular momentum,  $h$ , both computed in the inertial Galactic frame.

Since the permanence of bar-like structures in galaxies is a matter of debate, we cannot be sure that the bar of our Milky has existed throughout the Galactic lifetime. Therefore, we also ask ourselves how the orbits would look like if the bar has existed for only about a third of this lifetime.

To investigate the possible effects of spiral structure on the orbital characteristics of the clusters, we also include computations of the six globular clusters orbits in a Galactic potential that incorporates spiral arms. Among the six clusters selected for this computation, there is at least one cluster clearly belonging to the thick disk for which the effect of spiral perturbations is expected to be large (NGC 5927).

This paper is organized as follows. In Section 2 the Galactic potentials used to compute the cluster orbits are briefly described, and the initial conditions are presented. In Section 3 the orbits obtained with both the axisymmetric and the barred potential are presented and compared with the ones obtained by Casetti-Dinescu et al. (2007). In particular, we show that the effect of the bar is only negligible for one cluster NGC 3201, the most energetic one. We also discuss the effects on the orbits of a bar that has existed only during a fraction of the Galactic lifetime. In Section 4 the effect of spiral structure is presented for all six orbits. In Section 5 tidal radii are computed for orbits in the barred potential and compared with the axisymmetric case. Destruction rates for these clusters are also computed and discussed. The final Section 6 presents a brief discussion and our conclusions.

## 2. THE GALACTIC POTENTIALS AND THE INITIAL CONDITIONS

For our study we will employ the axisymmetric Galactic potential of Allen & Santillán (1991), the barred Galactic potential of Pichardo et al. (2004), and the bar-plus-spiral-arms model of Pichardo et al. (2003).

The bar model (for details see Pichardo et al. 2004) includes a bar of 3.13 kpc scale length, with axial ratios of 1.7:0.64:0.44, and a conservatively estimated mass of  $\sim 10^{10} M_{\odot}$  that replaces 70% of the spherical bulge mass. The bar moves with an angular velocity of  $60 \text{ km s}^{-1} \text{ kpc}^{-1}$ . This bar closely approximates Model S of Freudenreich (1998). Again, we use the superposition model of Pichardo et al. (2004).

To model the spiral perturbation we proceed as Pichardo et al. (2003), who refined their model until orbital self-consistent solutions were found. The spiral arms are constructed by using a three-dimensional mass distribution obtained by superposing oblate spheroidal potentials as building blocks of the global spiral potential. For an extensive description of the model see Pichardo et al. (2003). The adopted parameters are given in Section 4.

To calculate the initial conditions we take the absolute proper motions provided by Casetti-Dinescu et al. (2007). Other relevant data are taken from the compilation by Harris (1996). Once the space velocities are obtained, we integrate the orbits backwards in time for  $1.5 \times 10^{10}$  years. As in Paper I we analyze the time-reversed orbits. For the integration we use the Bulirsch-Stoer algorithm of Press et al. (1992). In the axisymmetric case the relative errors in the total energy were of about  $10^{-14}$  at the end of the integration. In the barred and spiral potential, the orbits are computed in the non-inertial reference frame where the bar is at rest. In the barred potential the precision of the calculations can be checked using Jacobi’s constant. The relative errors in this quantity turn out to be, typically,  $10^{-10}$  to  $10^{-11}$ .

## 3. THE GALACTIC ORBITS

Figure 1 shows the meridional orbits of the six clusters in both the axisymmetric and the barred potentials. Tables 1 and 2 summarize our results for both cases. In Table 1, corresponding to the axisymmetric potential, successive columns contain the name of the cluster, the minimum perigalactic distance reached in the course of the complete orbit, the average perigalactic distance, the maximum apogalactic distance, the average apogalactic distance, the maximum distance from the Galactic plane reached throughout the entire orbit, the average maximum distance from the Galactic plane, the average orbital eccentricity, the orbital energy per unit mass, the  $z$ -component of angular momentum per unit mass, two

values for the computed tidal radii (see discussion in Section 5), and the observed limiting radius, given in Harris (1996).

In Tables 1 and 2 two additional lines are given for each cluster. These correspond to “extreme” orbits, that take into account observational uncertainties. The meaning of these “extreme orbits” is discussed later in this section. Table 2, for the barred potential, is similar; but since neither the orbital energy,  $E$ , nor the  $z$ -component of angular momentum,  $h$  (both computed in the inertial Galactic frame) are constants of motion, we give in columns 9 and 10 the minimum and maximum values attained by  $h$  in the course of the complete orbit.

Only the orbit of NGC 3201, the least bound of the clusters, is not noticeably affected by the bar. The orbit remains entirely outside the bar region. This orbit closely resembles that of NGC 4590, presented in Paper I. As can be seen in Fig. 1, the orbits of the five remaining clusters are significantly affected by the bar. Their orbital parameters show fairly large changes as compared to the axisymmetric case, tending to reach higher values of apogalactic distance and distance to the Galactic plane, as well as becoming noticeably more irregular. They resemble the class of “inner” clusters studied in Paper I.

The orbits of NGC 4833 and NGC 5986 are irregular both without and with the bar. The orbit of NGC 2808 is near-resonant in the axisymmetric case, but it seems more irregular in the barred potential. The bar also causes the orbit to reach radii and  $z$ -distances larger than in the axisymmetric case. This orbit resembles that of NGC 6382, presented in our earlier study.

NGC 5927, a thick disk cluster, has a tightly confined box-type orbit in the axisymmetric case. The bar causes the orbit to extend to larger radial distances, reaching almost 7 kpc.

Finally, the orbit of NGC 4372, clearly near-resonant in the axisymmetric case, becomes irregular with the bar, and reaches larger  $z$ -distances.

Plots of the run of energy,  $E$ , and  $z$ -component of angular momentum,  $h$ , were obtained for all clusters. They are shown in Figures 2 and 3. These quantities are, of course, conserved in the axisymmetric case. In the presence of the bar, the orbits generally do not show large secular changes in  $E$  or  $h$ . Indeed, these quantities are conserved on the average within better than 10 percent. But periodic or quasi-periodic changes are seen to occur in all cases, reflecting the interactions with the bar. In Figures 2 and 3 we can see that NGC 3201, and NGC 5927 show small periodic or quasi-periodic changes. The occasional sudden changes we found in our previous study were found again for four of the six orbits here examined namely for NGC 2808, NGC 4372, NGC 4833 and NGC 5986. For this last cluster, the one with the smallest angular momentum, the abrupt changes in the angular momentum occasionally reverse the sense of revolution of the cluster around the Galactic center.

Figures 4 and 5 show plots of  $r_{min}$  and  $r_{max}$ , the minimum and maximum galactocentric distances attained by the six clusters during their time-reversed orbits in the barred potential. The figures show that these distances oscillate, particularly  $r_{max}$ . Clusters showing abrupt energy changes, like NGC 2808, NGC 4372, NGC 4833 and NGC 5986 also show changes in the oscillation of  $r_{max}$ ,  $r_{min}$ , and these occur at about the same times as the abrupt energy changes. Figure 6 shows a blowup of these oscillations for a short time at the beginning of the orbit computation of NGC 5927. The figure shows that the cluster attains the smaller  $r_{max}$  twice as often as the larger  $r_{max}$ . It reaches the smallest  $r_{min}$  twice as often as the larger  $r_{min}$ . This regular behavior is established right from the beginning of the orbit computation.

To obtain a very rough idea of the changes in the orbits that would appear if the Galactic bar were not a permanent feature, we computed the orbits backward in time, but only for the last 5.0 Gyr, that is, approximately a third of the Galactic lifetime. Figure 7 shows the orbits we obtained. A comparison of Figure 1 and Figure 7 clearly shows that the effects of the bar are quite similar for both cases. The sole exception is NGC 2808 whose orbit, when integrated backwards for only 5 Gyr, remains close to a resonance. We conclude that even if the Galactic bar has existed only for the last third of the Galactic lifetime, its effect on the orbits of the “inner” clusters is quite as noticeable as that of a bar present throughout the history of the Galaxy.

Of course, the bar is not expected to have suddenly come into existence 5 Gyr ago. A more realistic simulation would have to take into account the gradual formation of the bar (and perhaps even its gradual disappearance and re-formation). However, this kind of simulation is well beyond the scope of the present work. The issue of the origin and persistence of bars in galaxies is currently a subject of lively debate.

To assess the effects of observational uncertainties on the orbital parameters, we computed, as in Paper 1, two additional orbits for each cluster. The initial conditions for these orbits were chosen so as to maximize and minimize the orbital energy. In other words, we combined the observational uncertainties in such a way as to obtain two extreme orbits. Errors in the orbital parameters resulting from observational uncertainties are expected to be bounded by these extreme orbits, the real errors being expected to be much smaller. Indeed, note that the errors in the galactic parameters estimated by Casetti-Dinescu et al. (2007) for their orbits are much smaller than the ones that could be inferred from our extreme orbits.

A comparison of the values given in our Table 1 with the Galactic parameters obtained by Casetti-Dinescu et al. (2007) shows satisfactory overall agreement. In general, the uncertainties resulting from observational errors are larger than the ones resulting from using different axisymmetric Galactic potential models. However, our results on the orbits of the cluster “pairings” they find (NGC 5986-NGC 4833 and NGC 2808-NGC 4372) are not suffi-

ciently similar to make a convincing case for these “pairings”. The orbital parameters in the barred potential differ even more. So, we have to regard the “pairings” as not supported by the orbital parameters we obtain here.

## 4. THE EFFECTS OF SPIRAL ARM PERTURBATIONS

To study possible effects of spiral structure on the orbital characteristics of the clusters we computed some of the orbits using a Galactic potential that includes spiral arms. *A priori*, one would expect the effect of spiral structure to be small for two reasons: (a) the mass of the spiral features is small compared to that of the disk; (b) the great majority of the globular clusters spend most of their lifetimes away from the Galactic plane, and hence from the region of influence of the spiral arms. However, this is not the case for the thick-disk globular clusters. In this section we calculate the effect of spiral arms on the orbits of the six new clusters.

### 4.1. The Spiral Model

For the orbit computations we have used the semi-analytical model of Pichardo et al. (2003). This model is based on a three-dimensional mass distribution composed by the superposition of oblate spheroids as building blocks of the global spiral potential, rather than on a simple cosine law as it is customary. It provides a realistic representation of spiral features, particularly of flocculent arms.

To obtain a model matching current observational data we have updated the parameters used in Pichardo et al. (2003) according to recent observational work. In Pichardo et al. (2003) information on parameters not directly given by observations was completed by performing orbital calculations and searching for the most orbitally self-consistent model. The adopted features of the model we employ here are summarized as follows.

*The locus of the spiral arms.* The shape of the spiral arms is one of the few characteristics upon which almost all observations agree. In general, the spiral arms seem to be approximately logarithmic; for the Milky Way, in particular, this seems to be the case as shown in the very complete review by Vallée (2005a). We have taken the spiral locus given by Roberts et al. (1979), that combines a straight bar in the center of the Galaxy and a smoothly joined logarithmic region outwards.

*The number of spiral arms and the pitch angle.* We have taken the bisymmetric fit of Drimmel (2000) to the K-band of the COBE satellite, which has a pitch angle of  $i \sim 15.5^\circ$ .

Although observations in  $\text{-H}\alpha$  (Russeil et al. 2005), pulsar rotation measures (Vallée 2005b), radio observations of HII regions (Sewilo et al. 2004; Paladini et al. 2004), O and B stars (Negueruela & Marco 2003), near IR flux and gas (Bissantz et al. 2003), and ultra-compact HII regions seem to show a four-armed locus with a pitch angle  $i \sim 13.5^\circ$  (Vallée 2005a), we have assumed here that most of the mass is concentrated in the stellar arms as seen in the K-band (which traces the more massive old stellar population) rather than in the gaseous arms, which have been proposed as being the response of the gas to this two-armed stellar locus (Martos et al. 2004; Drimmel 2000). We expect that taking a two-armed structure instead of a four-armed one will provide a good (and conservative) estimate of the effects of this non-axisymmetric structure on the globular cluster orbits.

*Outer limit for the spiral arms.* We have based the adopted length of the spiral arms on observations rather than models. We have taken for this parameter a limiting galactocentric distance of  $R_f \sim 12$  kpc (Drimmel 2000; Caswell & Hanes 1987).

*Radial force produced by arms vs disk.* Patsis et al. (1991) built a family of self-consistent models and applied it to 12 normal spirals with known rotation curves and photometry. They found a correlation between the pitch angle and the ratio of the radial force of the arms to that of the axisymmetric disk. For a galaxy like the Milky Way, the pitch angles are in the range  $11^\circ$  to  $16^\circ$ , from which they obtained a force ratio of 4% to 10%. This corresponds in our model to a mass ratio of arms to disk of  $M_A/M_D = [2\%, 5\%]$ . Independently, models based on observations of our own Galaxy find a local force ratio of approximately 4% (Amaral & Lepine 1997). In our model we adopt a local force ratio of  $\sim 5\%$ , and a total mass for the bisymmetric spiral arms of  $M_A/M_D = 0.03$ .

*Angular velocity.* This is perhaps the most controversial dynamical parameter, due to the intrinsic difficulty of measuring it. Current observations and models, however, seem to show a trend, placing its value in the interval  $[20, 25]$   $\text{km s}^{-1} \text{kpc}^{-1}$ . Kinematic observations of stars of the local spiral arm, Orion, give  $\Omega = 25.7 \pm 1.2$   $\text{km s}^{-1} \text{kpc}^{-1}$  (Bobylev et al. 2006), whereas models (Martos et al. 2004; Pichardo et al. 2003) give  $\Omega = 20$   $\text{km s}^{-1} \text{kpc}^{-1}$ . We have taken for this work  $\Omega = 20$   $\text{km s}^{-1} \text{kpc}^{-1}$ .

## 4.2. The Orbits Perturbed by Spiral Arms

Although individual spiral arms may be transient structures in spiral galaxies, in fact the long-term effect of the spiral perturbation is likely to be important, since even if they were to last only a short time, they are soon replaced by new ones; this accounts for their ubiquity in the majority of disk galaxies. It has been customary to neglect the dynamical importance

of spiral arms based on empirical or intuitive arguments. Here we perform computations to study quantitatively their effects on the Galactic orbits, if any.

We integrated the six globular cluster orbits for the last 5 Gyr only, because, as we shall show, the effects of the spiral perturbation are already noticeable in this time span. The orbits are integrated in two variants of the potential, both including the axisymmetric potential (bulge, disk and halo). In one variant we added to the background axisymmetric potential the spiral arms, and in the other, the spiral arms and the bar.

In Figure 8 we show the results of the computations in the form of meridional orbits. The left panels refer to the orbits computed with the first variant of the potential, i.e. axisymmetric plus two-spiral-arm potential, and the right panels to the orbits in the second variant, i.e., axisymmetric plus bar plus two spiral arms. In all cases we analyze the orbits integrated backwards in time.

If we compare directly the orbits in the pure axisymmetric potential (Figure 7) with those in the potential with spiral arms (Figure 8), we can clearly see the effect of the spiral perturbation. The orbits change their shape in all cases, although only for clusters remaining closest to the Galactic plane (such as NGC 5927, NGC 4372, NGC 2808) the effect is noticeable. Again, the least affected orbits are those that reach large radial and vertical distances and remain mostly far from the influence of the arms, as is the case of NGC 3201. The orbit of this cluster is practically the same in all model potentials.

The effect of the spiral perturbation is most pronounced in the case of near-resonant (like that of NGC 2808), or irregular orbits (like NGC 4833 and NGC 5986). Indeed, NGC 2808 seems to get scattered out of its present near-resonance orbit more readily by the spiral perturbation than by the bar, a surprising result, since the mass of the bar is much larger. Another unexpected result is seen in the orbit of NGC 4833, which seems more symmetric with respect to the Galactic plane in the presence of the spiral perturbation.

As far as can be asserted on the basis of the six orbits here studied, the orbital parameters, such as the maximum absolute values of the  $z$ -distances and the peri- and apogalactic distances are not much affected by the presence of the spiral arms. The general tendency seems to be for the cluster orbits to have larger energies in the presence of spiral arms than in the axisymmetric case, and hence to attain larger apogalactic distances. This effect is largest for clusters remaining close to the Galactic plane ( $z \lesssim 2$  kpc), and inside the radial zone of strong influence of the spiral arms ( $3 < R < 8$  kpc). The combined effects of bar and spiral arm perturbations seem to be an efficient mechanism for attaining apogalactic distances larger than in the axisymmetric potential.

Even though in general the dynamical effects of the bar dominate over those of the

spiral arms, it is interesting to see that the spiral perturbations may play a non-negligible role. The clearest example is that of NGC 2808.

## 5. TIDAL RADII AND DESTRUCTION RATES

Ostriker et al. (1989) have emphasized the role played by a Galactic bar in selectively destroying clusters in box orbits passing near the Galactic center. In our present study, as well as in Paper I, we find that the smallest pericenters in the axisymmetric case (e.g. those of NGC 4833 and NGC 5986) tend to be larger in the presence of the bar. This is reflected in the destruction rates, which for these two clusters are sensibly smaller in the presence of the bar. Some possible reasons for this discrepancy are discussed in Paper I.

In the same manner as in Paper I, we have assessed the effects of the bar on the internal dynamics of the clusters and computed tidal radii and destruction rates.

For the six clusters we computed tidal radii using the King (1962) formula,  $r_K = [M_c/M_g(3 + e)]^{1/3}r_{min}$  with  $M_c$  the mass of the cluster,  $M_g$  an “effective Galactic mass”,  $e$  the orbital eccentricity, and  $r_{min}$  the galactocentric distance of a perigalactic point in the orbit. We have also calculated the tidal radius of each cluster using an alternative approximate formula introduced in Paper I, that has the advantage of not requiring an assumption about an “effective Galactic mass”, which is difficult to define if the perigalactic point lies in a region with a strong non-axisymmetric potential, as in the case of a bar. Our approximation is given by the equation

$$r_* = \left[ \frac{GM_c}{(\partial F_{x'}/\partial x')_{r'=0} + \dot{\theta}^2 + \dot{\varphi}^2 \sin^2 \theta} \right]^{1/3}, \quad (1)$$

where  $F_{x'}$  is the component of the Galactic acceleration along the line  $x'$  that joins the cluster with the Galactic center, and its partial derivative is evaluated at the position of the cluster. The angles  $\varphi$  and  $\theta$  are angular spherical coordinates of the cluster in an inertial Galactic frame. The tidal radius is computed at a perigalactic point in the orbit. In a two body problem  $r_*$  is reduced to King’s formula. For the derivation of the equation 1 see Appendix A of Paper I.

The last three columns of Table 1 contain  $r_K$ ,  $r_*$ , and  $r_L$  for the axisymmetric potential;  $r_L$  is the observed limiting radius of the cluster. In the last two columns of Table 2, we give  $r_K$  y  $r_*$  for the barred potential.

In Paper I we found that the formulae for  $r_*$  and  $r_K$  gave similar values. The same is

true for this new set of objects, independently of the potential variant employed (barred, barred plus spiral, or axisymmetric). This is shown in Figure 9, where we have taken the barred model as an example. In Figure 9 we show a comparison of the observed limiting radii ( $r_L$ ) with the theoretical ones; here using in particular King’s formula ( $r_K$ ).

The prograde-retrograde cluster NGC 5986 has a mean perigalactic distance that places it within the bar. Its tidal radius in Figure 10 lies under the line of coincidence, as was the case for most of the retrograde or prograde-retrograde clusters with a mean perigalactic distance of less than 3.5 kpc studied in Paper I. The only fully retrograde globular cluster of the new sample, NGC 3201, lies well above the line of coincidence but it is also the only cluster residing well outside the bar. For a discussion of the importance of the orbital sense (prograde or retrograde) on the tidal radii we refer the reader to Section 4 of Paper I.

Regarding the destruction rates, we have calculated the time of destruction due to components of bulge and disk in the Galaxy based on the results of several papers on the subject (Aguilar et al. 1988; Long et al. 1992; Gnedin & Ostriker 1997,1999; Spitzer 1987; Kundić & Ostriker 1995; Gnedin et al. 1999a,b). As in Paper I, we define the total destruction rate due to gravitational shocks with the bulge as

$$\frac{1}{t_{bulge}} = \frac{1}{t_{bulge,1}} + \frac{1}{t_{bulge,2}} \quad (2)$$

where

$$t_{bulge,1} = \left( \frac{-E_c}{\langle (\Delta E)_b \rangle} \right) P_{orb}, \quad (3)$$

$$t_{bulge,2} = \left( \frac{E_c^2}{\langle (\Delta E)_b^2 \rangle} \right) P_{orb}, \quad (4)$$

with  $E_c \simeq -0.2GM_c/r'_h$  the mean binding energy per unit mass of the cluster and  $P_{orb}$  its orbital period in the Galactic radial direction.

In the same manner, for the disk we have the total destruction rate due to gravitational shocks,

$$\frac{1}{t_{disk}} = \frac{1}{t_{disk,1}} + \frac{1}{t_{disk,2}}, \quad (5)$$

where

$$t_{disk,1} = \left( \frac{-E_c}{\langle (\Delta E)_d \rangle} \right) \frac{P_{orb}}{n}, \quad (6)$$

$$t_{disk,2} = \left( \frac{E_c^2}{\langle (\Delta E)_d^2 \rangle} \right) \frac{P_{orb}}{n}. \quad (7)$$

Here,  $n$  is the number of crossings with the disk during the radial orbital period  $P_{orb}$ . For a summary on destruction rate formulae see Paper I.

We have applied these formulae to the six globular clusters and to the specific case including a Galactic bar. It is worth noting that we have taken very conservative values for the mass and radius for the Galactic bar. According to recent estimates the bar could extend at least 1 kpc beyond the limit we used (López-Corredoira et al. 2007), and it could have at least twice the observed mass if it is combined with the response of a dark matter halo, which apparently produces a dark bar aligned with the visible one (Colín et al. 2006; Athanassoula 2007); thus the effect of the bar might be considerably stronger.

In Table 3 we present the destruction rates obtained in our computations. The first column shows the name of the cluster. The second column gives the mass of the cluster, computed with a mass-to-light ratio of 2. Absolute visual magnitudes are taken from Harris (1996). The central concentration and the half-mass radius are given in columns three and four, and are taken from Harris (1996).

The remaining columns show the destruction rates due to the bulge and disk. These destruction rates are the averages over the last  $10^9$  yr in a cluster’s orbit, taking the corresponding perigalactic points and crossings with the Galactic disk. For a given cluster, the first line in Table 3 shows the destruction rates computed in the axisymmetric potential; the second line gives the corresponding values in the barred potential.

The new sample resides much closer to the Galactic disk than did most of the 48 clusters of Paper I. NGC 3201 and NGC 2808 show the longest total destruction times, taking both disk and bulge into account. The difference between the barred and non-barred models is largest for NGC 5986, NGC 4833, whose orbits lie almost entirely within the bar, and are thus the most affected by it. Also affected though not as much, are NGC 5927 that resides in the outskirts of the bar but very close to the Galactic plane, and NGC 4372 whose average apocenter lies inside the bar.

In Figure 11 we plot only the values obtained with the ‘central orbits’. This figure shows that the destruction rates due to the bulge depend on the mean perigalactic distance, both for the axisymmetric potential (Frame a) and for the barred potential (Frame c). Clusters

with perigalactic points close to the Galactic center and large orbital eccentricities (squares marked with a circle) have, in general, greater bulge destruction rates. Frames (b) and (d) of Figure 11 show the comparison of the destruction rates due to the bulge and disk, in the axisymmetric and in the barred potential, respectively. These frames show that bulge shocking dominates in the bar region, as found by Aguilar et al. (1988). We confirm as in Paper I that the destruction rates are very similar in both the axisymmetric and the barred Galactic potential.

In this study we have found that the bar is the most important non-axisymmetric structure in the Galaxy as regards its orbital effects, tidal radii and destruction rates of globular clusters. The spiral arms produce small, though non-negligible effects in the orbits of the clusters moving closest to the Galactic plane (see Section 4.2). Since the changes in destruction rates and tidal radii depend mainly on the orbital parameters, the effects of the spiral arms in a Milky-Way-like galaxy are negligible compared to the effects of the bar. However, in the case of grand-design spirals or of galaxies with a weak bar or entirely without bar, the effects of the spiral arms should not be considered to be negligible.

## 6. DISCUSSION AND CONCLUSIONS

We have obtained orbits for 6 additional globular clusters in both a barred and an axisymmetric Galactic potential, as well as in models including spiral arms. The total number of clusters with available orbits is now 54. Among the newly calculated cases, only the orbit of NGC 3201, an “outer” cluster, is unaffected by the bar. The other five clusters have orbits residing within the region of influence of the bar, and their orbits are clearly influenced by it. As in our previous study, we find that the main changes the bar causes in the orbits are larger vertical and radial excursions, and far more irregular orbits. In general, the bar causes no net global changes in the energy or the  $z$ -component of the angular momentum, computed in an inertial frame. However, in four out of the six cases, jumps in these quantities do occur, even causing a temporary reversal of the sense of rotation of the orbit in the case of NGC 5986. The effect of a shorter-lived bar is found to be quite as noticeable on these orbits as that of the longer-lived one.

Orbits with spiral-arm perturbations were also computed. Contrary to expectations, even a small perturbation, accounting for only 5% of the local radial force ratio arm-disk, causes significant changes in the form of the orbits. Although the influence of the spiral arms on the orbits of the clusters closest to the Galactic disk are not negligible, the long-term effects are definitely dominated by the Galactic bar.

Tidal radii have been computed with the expression derived in Paper I, as well as with a numerical evaluation of the relevant quantities along the orbit. Again, we found little change due to the bar. When changes did occur, they again make the computed tidal radii somewhat larger in the presence of a bar. With the new material on hand, we confirm our earlier finding that the destruction rates due to shocks with the Galactic bulge and disk are not strongly affected when we consider a barred Galactic potential, or a barred potential with spiral arm perturbations.

### **Acknowledgments**

B.P. thankfully acknowledges the support of CONACyT, Mexico, through grant 50720.

## REFERENCES

- Aguilar, L., Hut, P., & Ostriker, J. P. 1988, *ApJ*, 335, 720
- Allen, C.; Moreno, E.; Pichardo, B., 2006 *ApJ*, 652, 1150 (Paper I)
- Allen, Christine; Poveda, Arcadio; Hernández-Alcantara, A. Proceedings of IAU Symposium 240, Edited by W.I. Hartkopf, E.F. Guinan and P. Harmanec. Cambridge: Cambridge University Press, 2007., pp.405-413 (arXiv:astro-ph/0611789)
- Allen, C., & Santillán, A. 1991, *Rev. Mexicana Astron. Astrofis.*, 22, 255
- Amaral, L. H.; Lepine, J. R. D. 1997, *MNRAS*, 286, 885
- Athanassoula, E. 2007, *MNRAS*, 377, 1569
- Bissantz, Nicolai; Englmaier, Peter; Gerhard, Ortwin. 2003, *MNRAS*, 340, 949
- Bobylev, V. V.; Goncharov, G. A.; Bajkova, A. T. 2006, *ARep*, 50, 733
- Casetti-Dinescu, Dana I.; Girard, Terrence M.; Herrera, David; van Altena, William F.; López, Carlos E.; Castillo, Danilo J. 2007, *AJ*, 134, 195
- Caswell, J. L.; Haynes, R. F. 1987, *A&A*, 171, 261
- Colín, P., Valenzuela, O., & Klypin, A. 2006, *ApJ*, 644, 687
- Drimmel, R. 2000, *A&A*, 358L, 13
- Freudenreich, H. T. 1998, *ApJ*, 492, 495
- Gnedin, O. Y., & Ostriker, J. P. 1997, *ApJ*, 474, 223
- Gnedin, O. Y., & Ostriker, J. P. 1999, *ApJ*, 513, 626
- Gnedin, O. Y., Hernquist, L., & Ostriker, J. P. 1999, *ApJ*, 514, 109
- Gnedin, O. Y., Lee, H. M., & Ostriker, J. P. 1999, *ApJ*, 522, 935
- Harris, W. E. 1996, *AJ*, 112, 1487
- Kepley, Amanda A.; Morrison, Heather L.; Helmi, Amina; Kinman, T. D.; Van Duyne, Jeffrey; Martin, John C.; Harding, Paul; Norris, John E.; Freeman, Kenneth C. 2007, *AJ*, 134, 1579
- King, I. R. 1962, *AJ*, 67, 471

- Kundić, T., & Ostriker, J. P. 1995, *ApJ*, 438, 702
- Long, K., Ostriker, J. P., & Aguilar, L. 1992, *ApJ*, 388, 362
- Martos, M.; Hernández, X.; Yáñez, M.; Moreno, E.; Pichardo, B. 2004, *MNRAS*, 350, 47
- López-Corredoira, M.; Cabrera-Lavers, A.; Mahoney, T. J.; Hammersley, P. L.; Garzón, F.; González-Fernández, C. 2007, *AJ*, 133, 154
- Negueruela, I.; Marco, A. 2003, *A&A*, 406, 119
- Ostriker, J.P., Binney, J., Saha, P. 1989, *MNRAS*, 241, 849.
- Paladini, R.; Davies, R. D.; DeZotti, G. 2004, *MNRAS*, 347, 237
- Patsis, P. A.; Contopoulos, G.; Grosbol, P. 1991, *A&A*, 243, 373
- Pichardo, B., Martos, M., & Moreno, E. 2004, *ApJ*, 609, 144
- Pichardo, B., Martos, M., & Moreno, E., Espresate, J., 2003, *ApJ*, 582, 230
- Press, W. H., Teukolsky, S. A., Vetterling, W. T., & Flannery, B. P., 1992, *Numerical Recipes in Fortran 77: The Art of Scientific Computing* (2nd ed.; Cambridge: Cambridge Univ. Press)
- Roberts, W. W., Jr.; Huntley, J. M.; van Albada, G. D. 1979, *ApJ*, 233, 67
- Russeil, D.; Adami, C.; Amram, P.; Le Coarer, E.; Georgelin, Y. M.; Marcelin, M.; Parker, Q. 2005, *A&A*, 429, 497
- Sewilo, M.; Churchwell, E.; Kurtz, S.; Goss, W. M.; Hofner, P. 2004, *ApJ*, 605, 285
- Spitzer, L., 1987, *Dynamical Evolution of Globular Clusters* (Princeton: Princeton Univ. Press)
- Vallée, J. P. 2005, *AJ*, 130, 569
- Vallée, J. P. 2005, *ApJ*, 619, 297

Table 1. Orbits with the axisymmetric potential

Cluster	$(r_{min})_{min}$ (kpc)	$\langle r_{min} \rangle$ (kpc)	$(r_{max})_{max}$ (kpc)	$\langle r_{max} \rangle$ (kpc)	$( z _{max})_{max}$ (kpc)	$\langle  z _{max} \rangle$ (kpc)	$\langle e \rangle$	$E$ ( $10\text{kms}^{-1}$ ) <sup>2</sup>	$h$ ( $10\text{kms}^{-1}\text{kpc}$ )	$r_K$ (pc)	$r_*$ (pc)	$r_L$ (pc)
NGC 2808	2.65	2.76	12.86	12.72	4.42	2.60	0.643	-1192.93	87.32	56.3	54.3	43.4
	1.88	2.10	11.82	11.48	4.86	2.38	0.691	-1241.68	68.36	48.7	46.1	
	3.67	3.89	13.83	13.81	5.89	3.95	0.560	-1134.84	112.24	72.7	73.0	
NGC 3201	9.26	9.31	27.02	26.99	8.97	5.95	0.487	-841.75	-278.09	72.0	73.4	41.4
	9.03	9.08	22.99	22.96	7.15	4.99	0.433	-895.62	-262.22	70.6	73.4	
	9.50	9.56	31.99	31.97	11.24	7.15	0.540	-784.32	-295.27	73.0	73.4	
NGC 4372	2.91	2.93	7.88	7.74	2.06	1.74	0.451	-1377.43	83.03	37.5	38.6	58.8
	1.99	2.04	7.72	7.62	1.64	1.35	0.578	-1416.52	64.81	29.0	28.3	
	4.06	4.22	7.74	7.74	2.89	2.37	0.294	-1330.13	102.25	48.2	52.8	
NGC 4833	0.19	0.68	8.92	8.08	6.02	1.80	0.847	-1410.26	11.04	15.8	14.7	33.8
	0.01	0.76	8.13	6.71	6.31	3.32	0.808	-1453.00	0.33	13.1	11.3	
	0.48	0.96	9.80	9.06	5.82	2.05	0.811	-1355.97	25.27	18.4	17.1	
NGC 5927	4.70	4.72	5.76	5.74	0.84	0.80	0.098	-1422.14	107.14	52.1	61.5	36.9
	3.85	3.85	5.46	5.46	0.67	0.62	0.172	-1479.97	93.17	45.5	52.9	
	4.68	4.71	7.41	7.39	1.23	1.08	0.222	-1344.77	119.58	51.3	58.2	
NGC 5986	0.08	0.82	5.67	4.44	3.97	1.98	0.694	-1622.48	4.04	15.1	14.5	31.8
	0.00	0.67	4.98	3.83	3.61	1.92	0.714	-1681.18	0.00	16.5	16.1	
	0.99	1.07	5.93	5.79	2.88	1.74	0.688	-1545.02	17.96	21.0	20.8	

Table 2. Orbits with the barred potential

Cluster	$(r_{min})_{min}$ (kpc)	$\langle r_{min} \rangle$ (kpc)	$(r_{max})_{max}$ (kpc)	$\langle r_{max} \rangle$ (kpc)	$( z _{max})_{max}$ (kpc)	$\langle  z _{max} \rangle$ (kpc)	$\langle e \rangle$	$h_{min}$ ( $10\text{kms}^{-1}\text{kpc}$ )	$h_{max}$ ( $10\text{kms}^{-1}\text{kpc}$ )	$r_K$ (pc)	$r_*$ (pc)
NGC 2808	2.37	2.86	15.63	13.27	5.67	2.92	0.645	77.67	101.11	57.0	56.0
	1.40	1.82	12.83	11.33	5.17	1.54	0.723	55.01	79.13	42.5	39.9
	3.35	3.93	14.31	11.99	6.21	3.97	0.505	93.15	114.73	72.4	73.0
NGC 3201	9.26	9.31	26.99	26.96	8.96	5.94	0.487	-278.21	-278.03	71.9	73.4
	9.03	9.07	22.97	22.94	7.14	4.98	0.433	-262.34	-262.15	70.6	73.3
	9.50	9.56	31.97	31.94	11.23	7.15	0.539	-295.39	-295.22	72.9	73.4
NGC 4372	1.91	2.65	8.03	6.60	3.04	1.59	0.428	47.37	88.84	35.2	37.2
	1.41	1.78	7.67	6.91	3.23	1.09	0.590	47.27	69.36	28.0	27.8
	3.48	3.92	9.61	7.64	3.36	2.09	0.317	85.32	112.12	43.7	46.7
NGC 4833	0.19	0.79	10.56	8.66	5.85	1.78	0.835	0.96	30.57	20.2	17.5
	0.14	0.81	11.85	8.83	5.96	2.04	0.833	-4.71	37.21	17.6	14.5
	0.36	1.19	11.25	9.28	6.35	2.60	0.777	10.32	41.41	20.8	18.6
NGC 5927	4.28	4.47	6.64	5.98	0.90	0.79	0.144	103.19	112.55	49.8	57.6
	0.83	2.64	7.26	4.32	0.63	0.45	0.252	23.67	108.04	28.3	32.4
	4.67	4.70	7.67	7.50	1.25	1.09	0.229	117.90	121.30	51.5	58.5
NGC 5986	0.03	0.60	6.50	5.21	3.53	1.23	0.795	-6.80	19.94	20.0	19.4
	0.02	0.58	5.60	4.45	3.03	1.05	0.775	-20.88	16.90	19.4	18.8
	0.10	0.90	6.69	5.10	4.14	1.90	0.708	-9.40	26.12	23.3	22.7

Table 3. Destruction Rates

Cluster	$M_c$ ( $M_\odot$ )	$c$	$r_h$ ( $pc$ )	$\langle 1/t_{bulge,1} \rangle$ ( $yr^{-1}$ )	$\langle 1/t_{bulge,2} \rangle$ ( $yr^{-1}$ )	$\langle 1/t_{bulge} \rangle$ ( $yr^{-1}$ )	$\langle 1/t_{disk,1} \rangle$ ( $yr^{-1}$ )	$\langle 1/t_{disk,2} \rangle$ ( $yr^{-1}$ )	$\langle 1/t_{disk} \rangle$ ( $yr^{-1}$ )
NGC 2808	9.7E05	1.77	2.12	9.5E-15	6.3E-16	1.0E-14	4.4E-14	3.5E-15	4.7E-14
				6.9E-15	4.5E-16	7.3E-15	3.3E-14	2.7E-15	3.6E-14
NGC 3201	1.6E05	1.30	3.90	8.1E-17	8.1E-18	8.9E-17	2.8E-15	3.9E-16	3.2E-15
				8.1E-17	8.2E-18	9.0E-17	2.8E-15	3.9E-16	3.2E-15
NGC 4372	2.2E05	1.30	6.58	3.1E-12	7.2E-13	3.9E-12	2.2E-11	6.3E-12	2.9E-11
				5.1E-12	1.2E-12	6.3E-12	2.7E-11	7.8E-12	3.5E-11
NGC 4833	3.1E05	1.25	4.56	2.5E-10	1.0E-10	3.5E-10	1.6E-12	4.8E-13	2.1E-12
				4.3E-11	1.7E-11	6.0E-11	1.3E-12	4.2E-13	1.7E-12
NGC 5927	2.2E05	1.60	2.54	6.8E-16	5.0E-17	7.3E-16	7.2E-13	7.3E-14	8.0E-13
				1.9E-15	1.5E-16	2.1E-15	8.0E-13	8.2E-14	8.8E-13
NGC 5986	4.1E05	1.22	3.18	4.8E-10	1.6E-10	6.4E-10	1.4E-12	3.0E-13	1.7E-12
				2.2E-11	5.0E-12	2.7E-11	1.4E-12	2.7E-13	1.7E-12

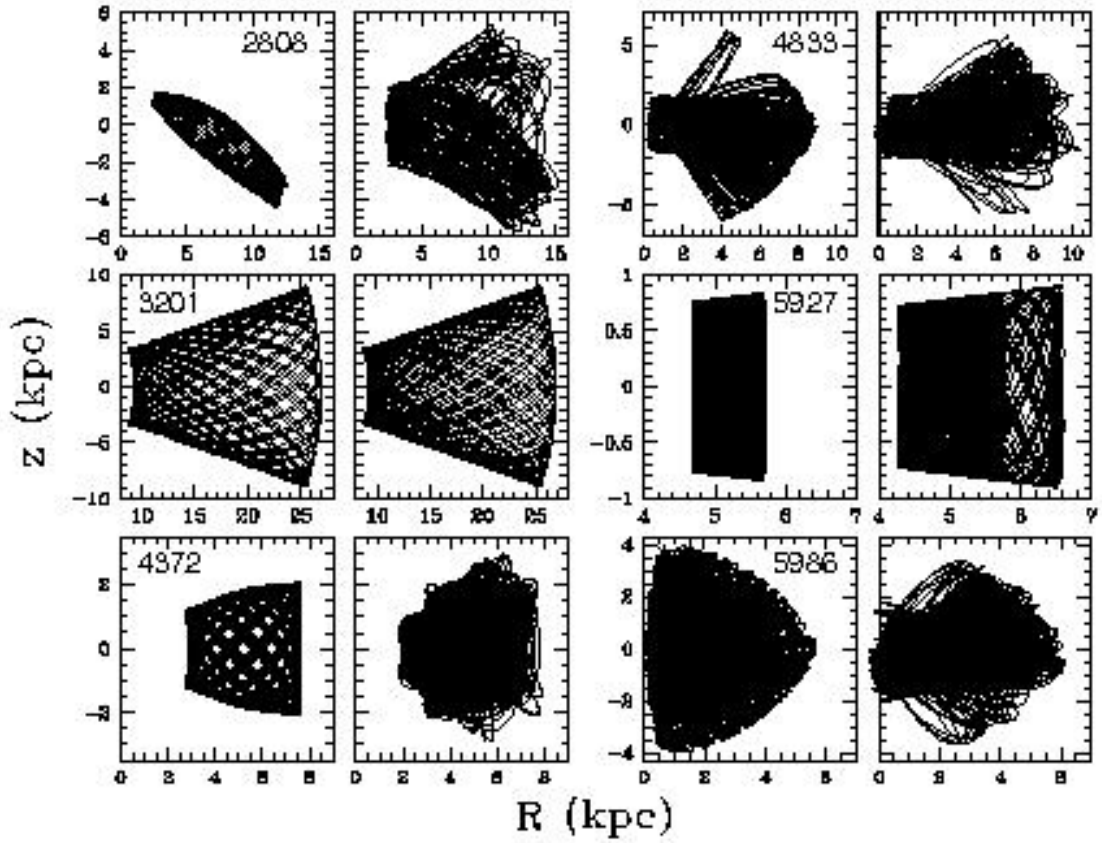


Fig. 1.— Meridional Galactic orbits of the six clusters during the lifetime of the Galaxy. For each cluster, the orbits in the axisymmetric (left) and barred (right) potentials are shown.

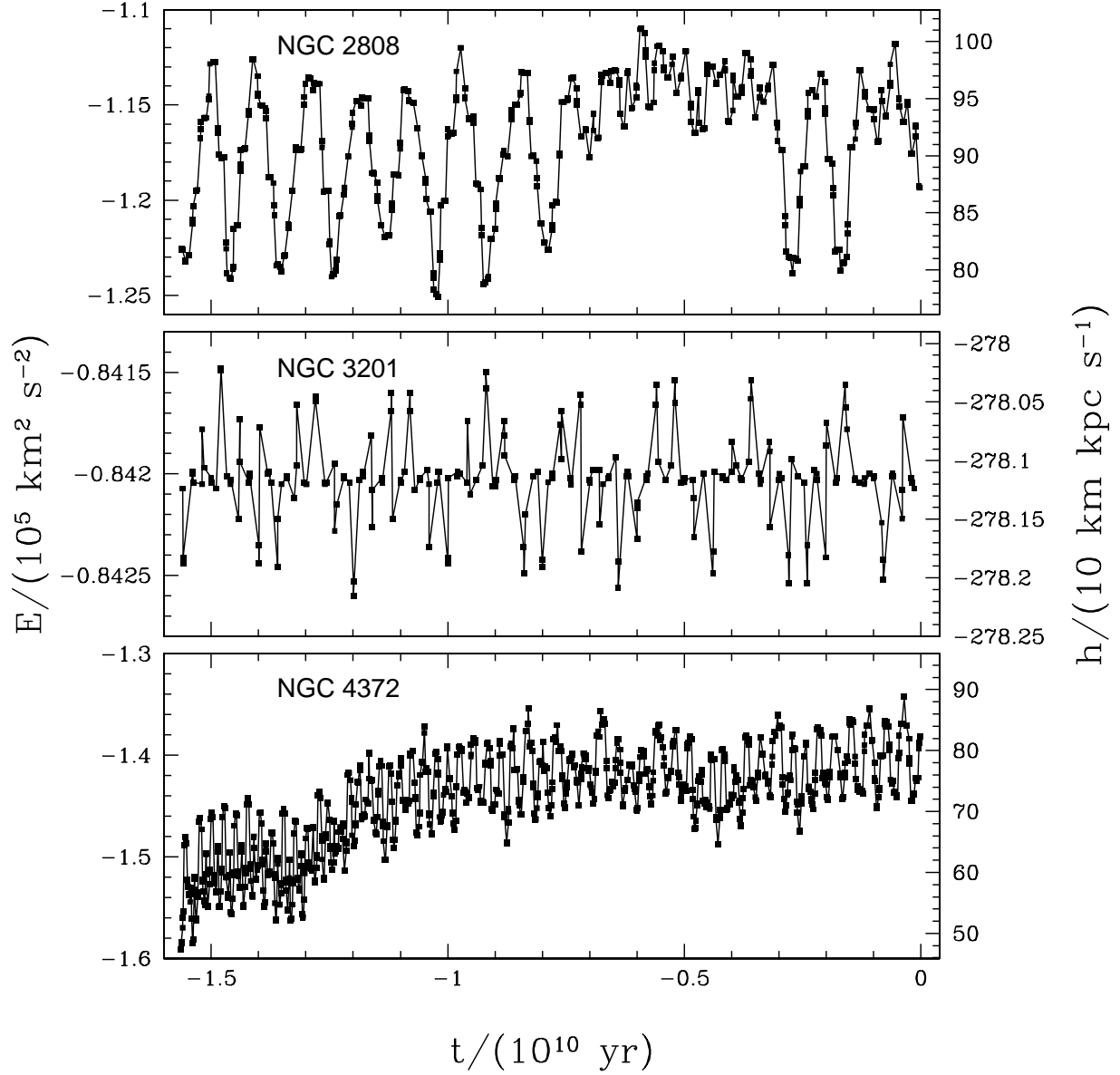


Fig. 2.— Energy and  $z$ -angular momentum as functions of time in NGC 2808, NGC 3201, and NGC 4372, with the barred potential.

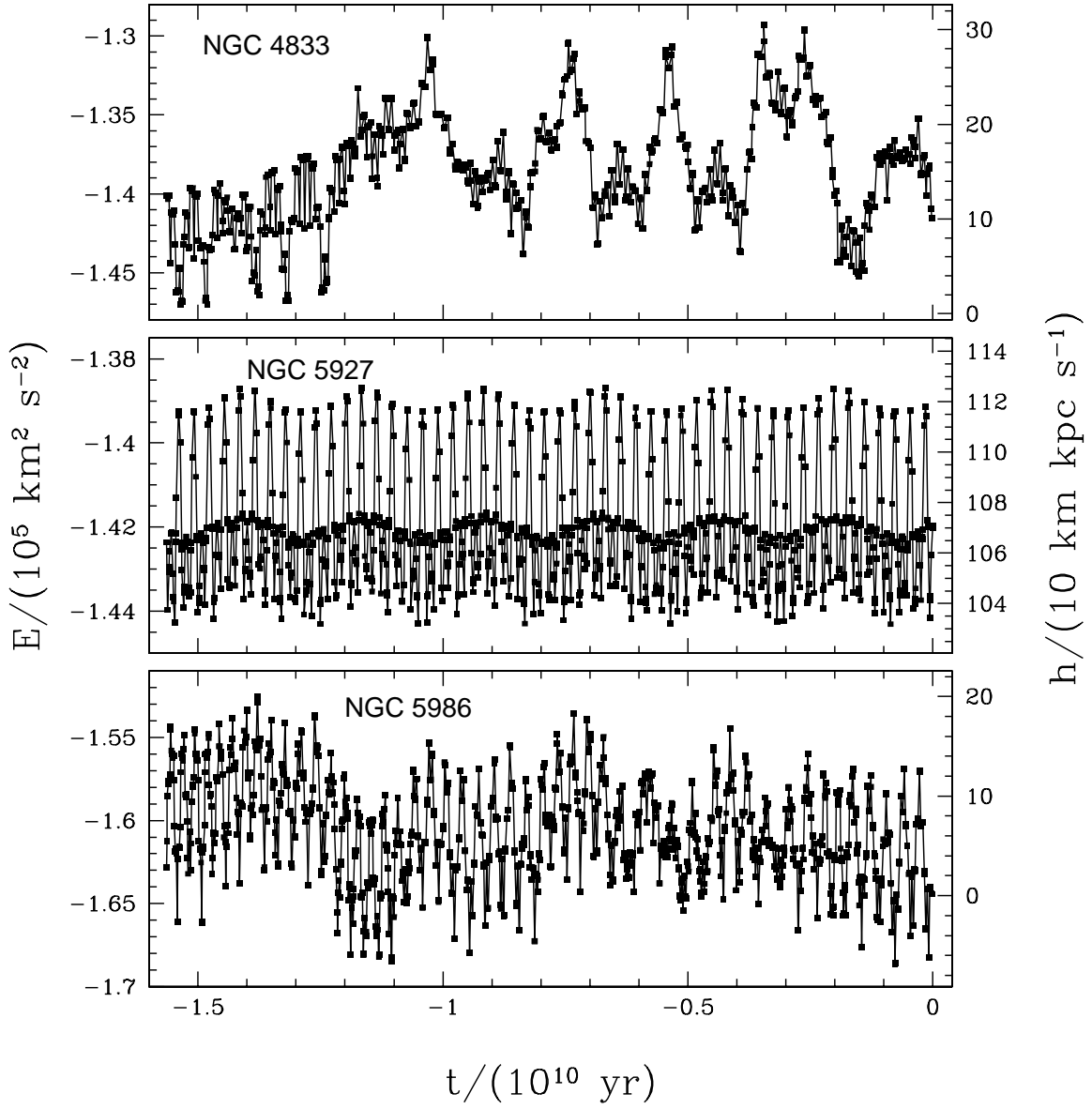


Fig. 3.— As in Figure 2, for NGC 4833, NGC 5927, and NGC 5986.

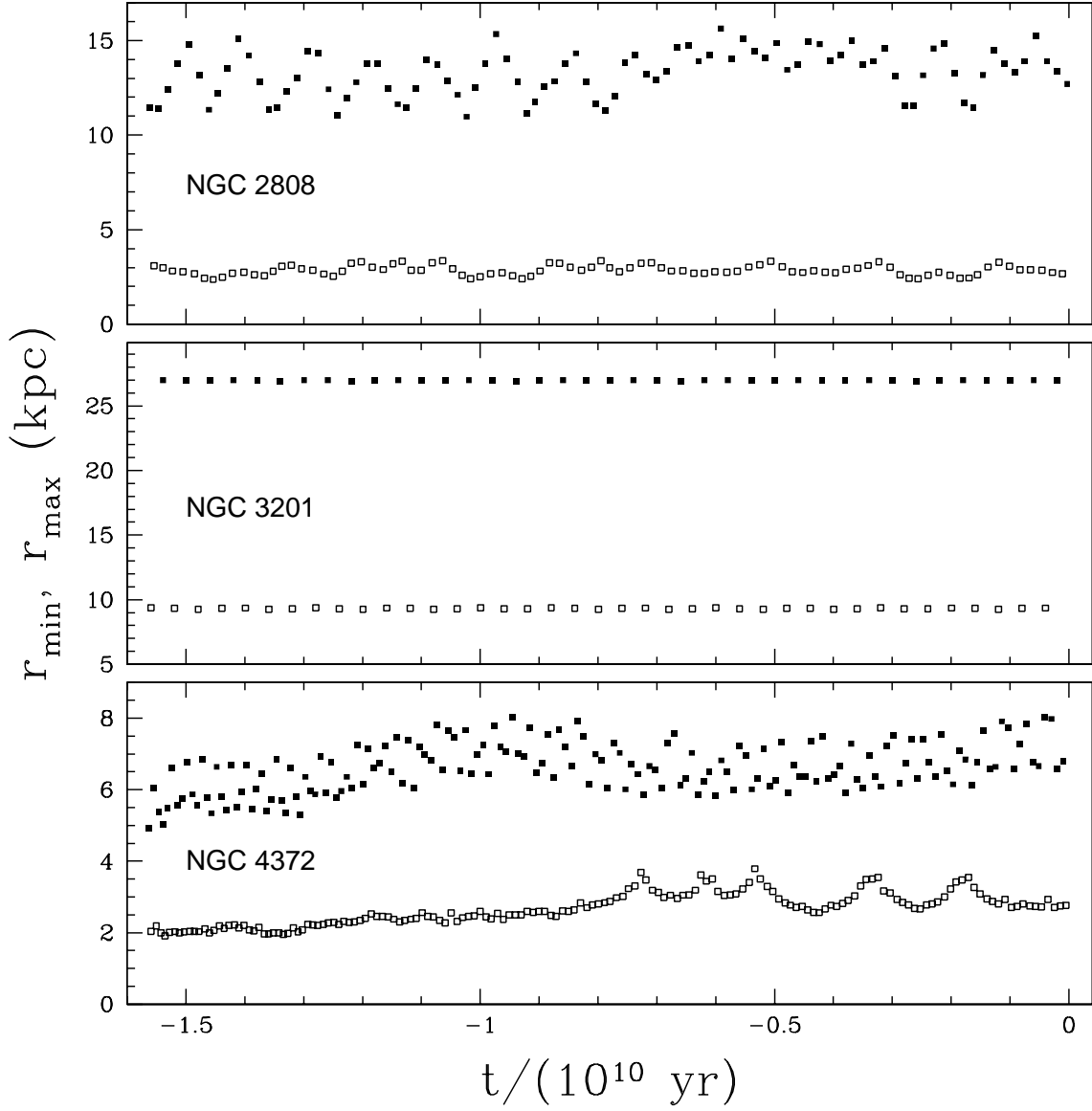


Fig. 4.— Galactocentric distances  $r_{\min}$  (empty squares) and  $r_{\max}$  (filled squares) in NGC 2808, NGC 3201, and NGC 4372.

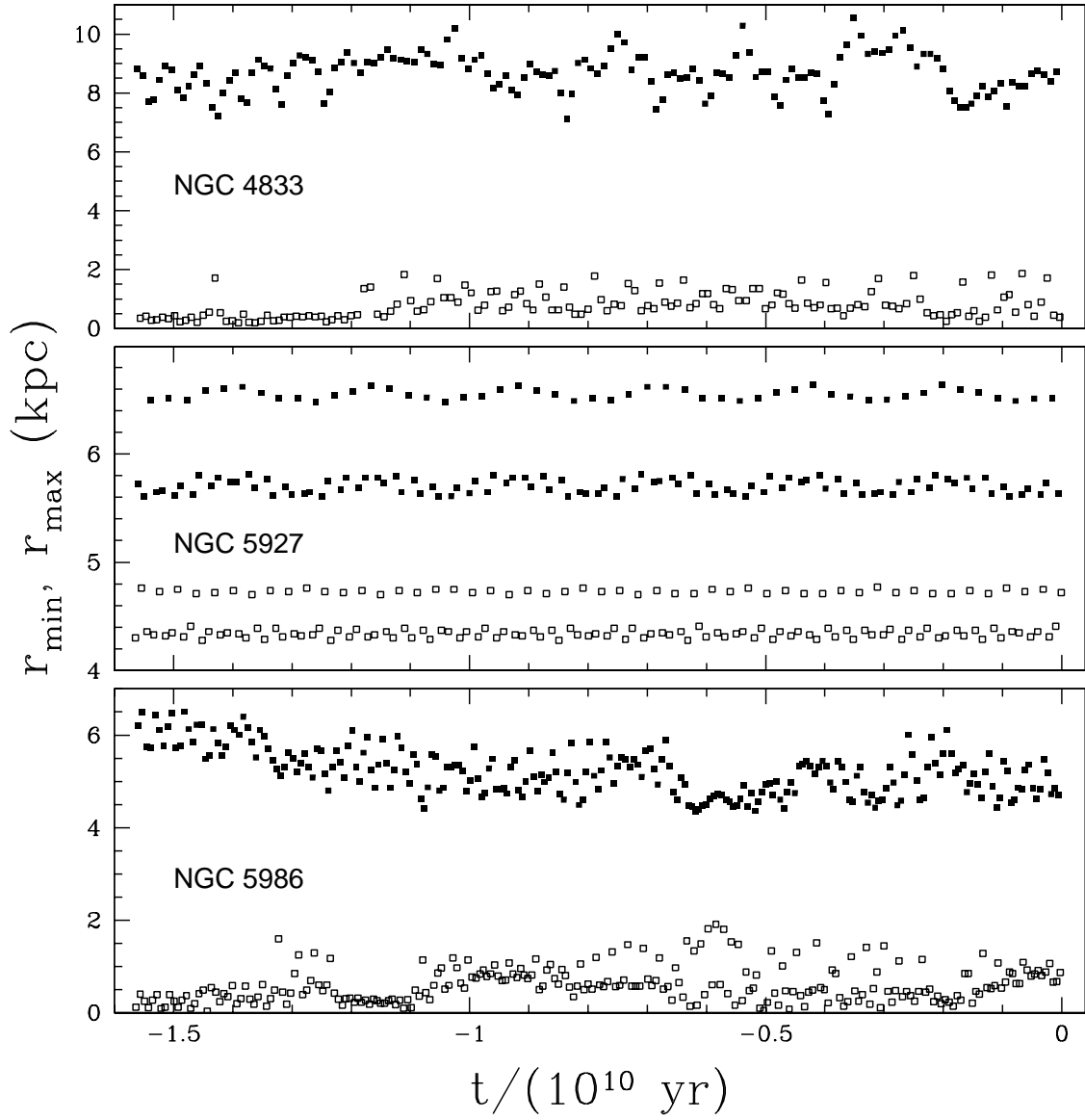


Fig. 5.— As in Figure 4, for NGC 4833, NGC 5927, and NGC 5986.

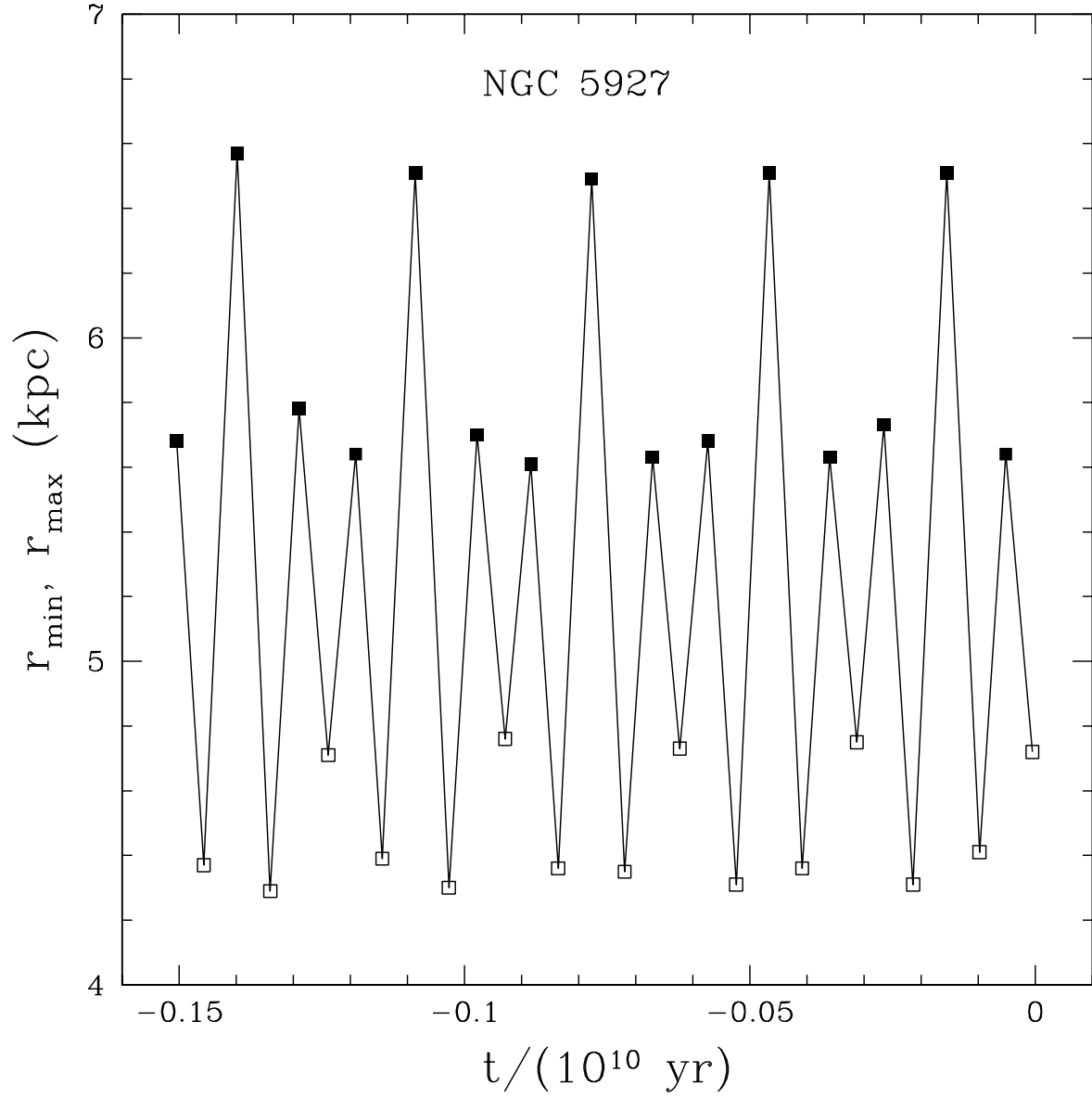


Fig. 6.— Detail around  $t = 0$  of the middle frame in Figure 5 for NGC 5927. The continuous line connects successive  $r_{\min}$  and  $r_{\max}$ .

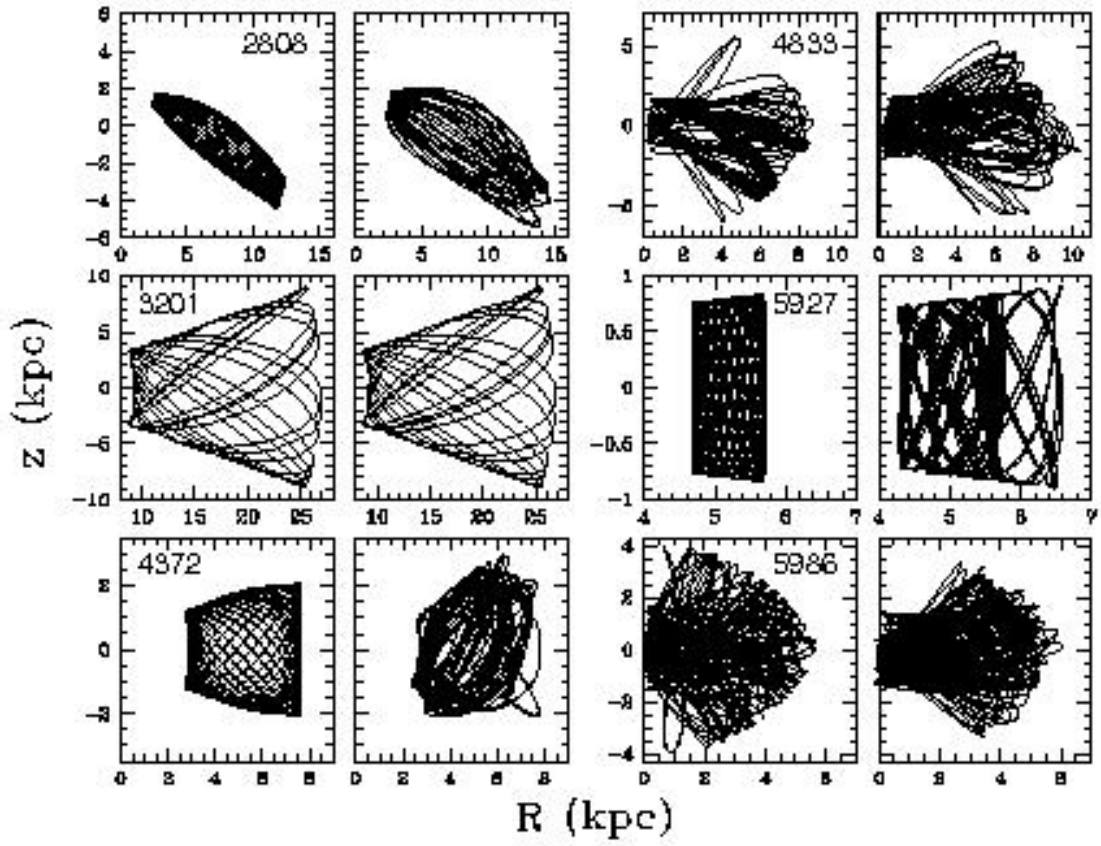


Fig. 7.— As in Figure 1, now for the last 5 Gyr.

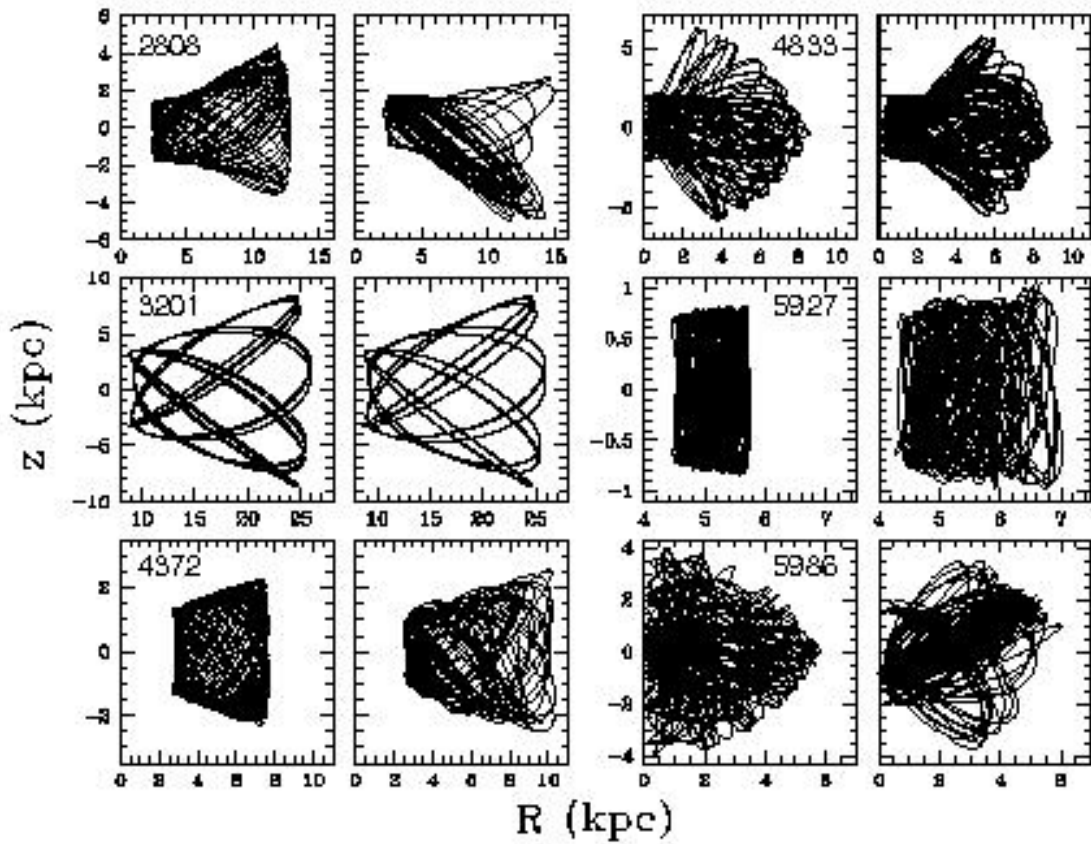


Fig. 8.— The effect of the spiral arms. Meridional Galactic orbits of the six clusters during the last 5 Gyr. For each cluster, the left frame shows the orbit in the axisymmetric plus the two-spiral-arm potential, and the right frame shows the orbit in the barred (axisymmetric + bar potential) plus the two-spiral-arm potential.

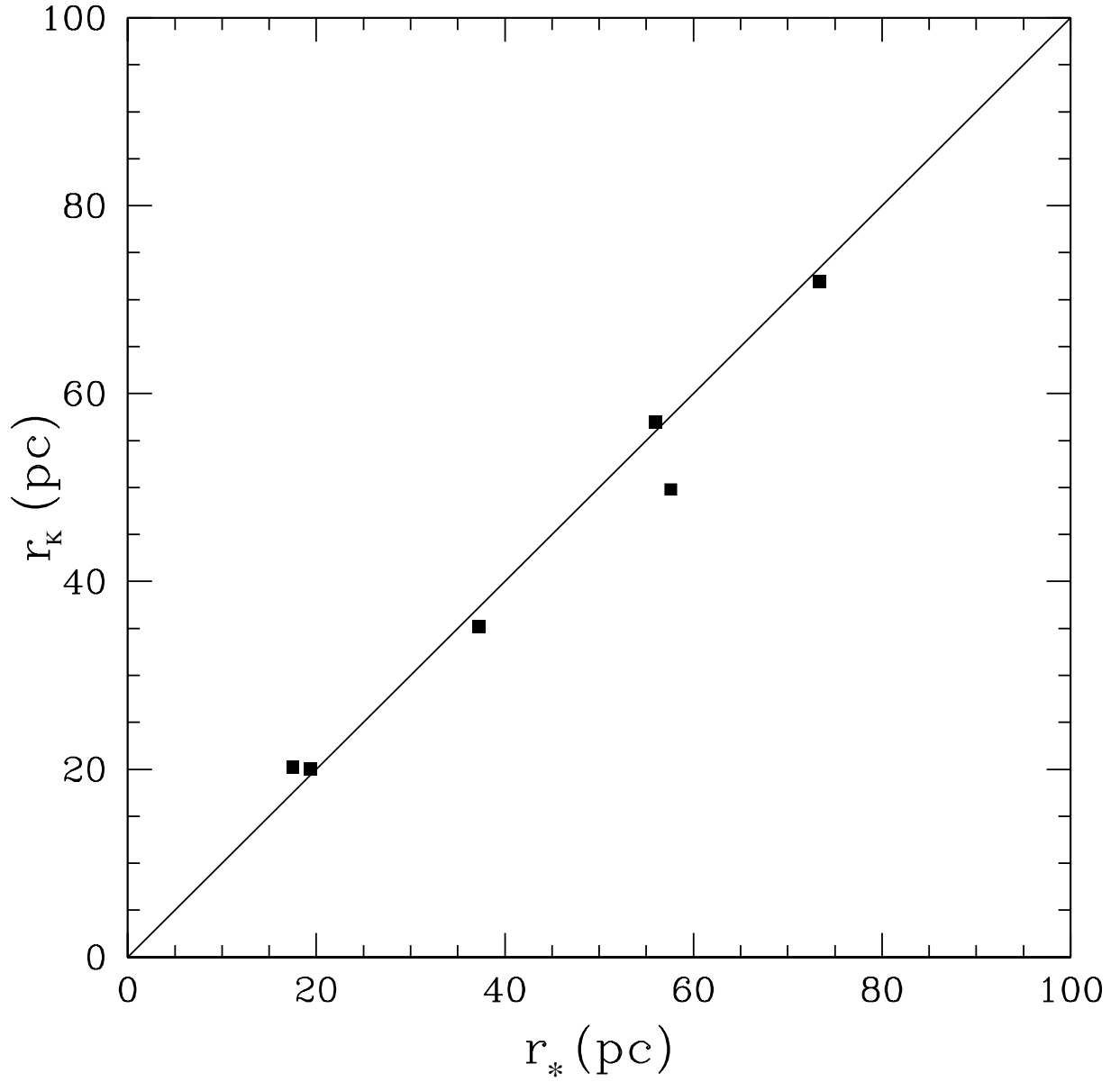


Fig. 9.— Comparison of tidal radii  $r_k$  and  $r_*$  using the non-axisymmetric (barred) potential. The line is the line of coincidence.

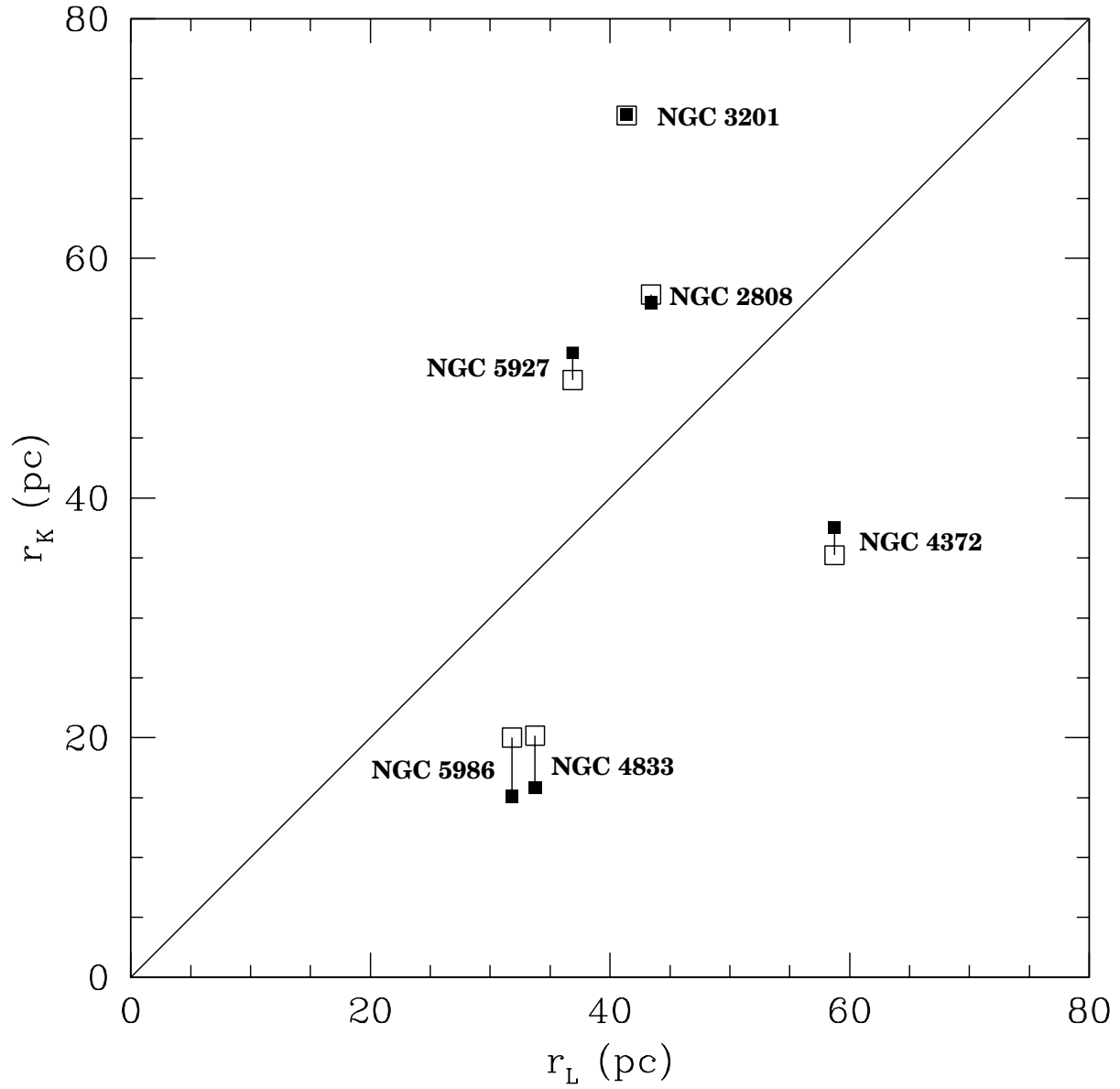


Fig. 10.— Tidal radius  $r_K$  (King) compared with the observed limiting radius  $r_L$ . Results with the axisymmetric (filled squares), and barred (empty squares) potentials. The line is the line of coincidence.

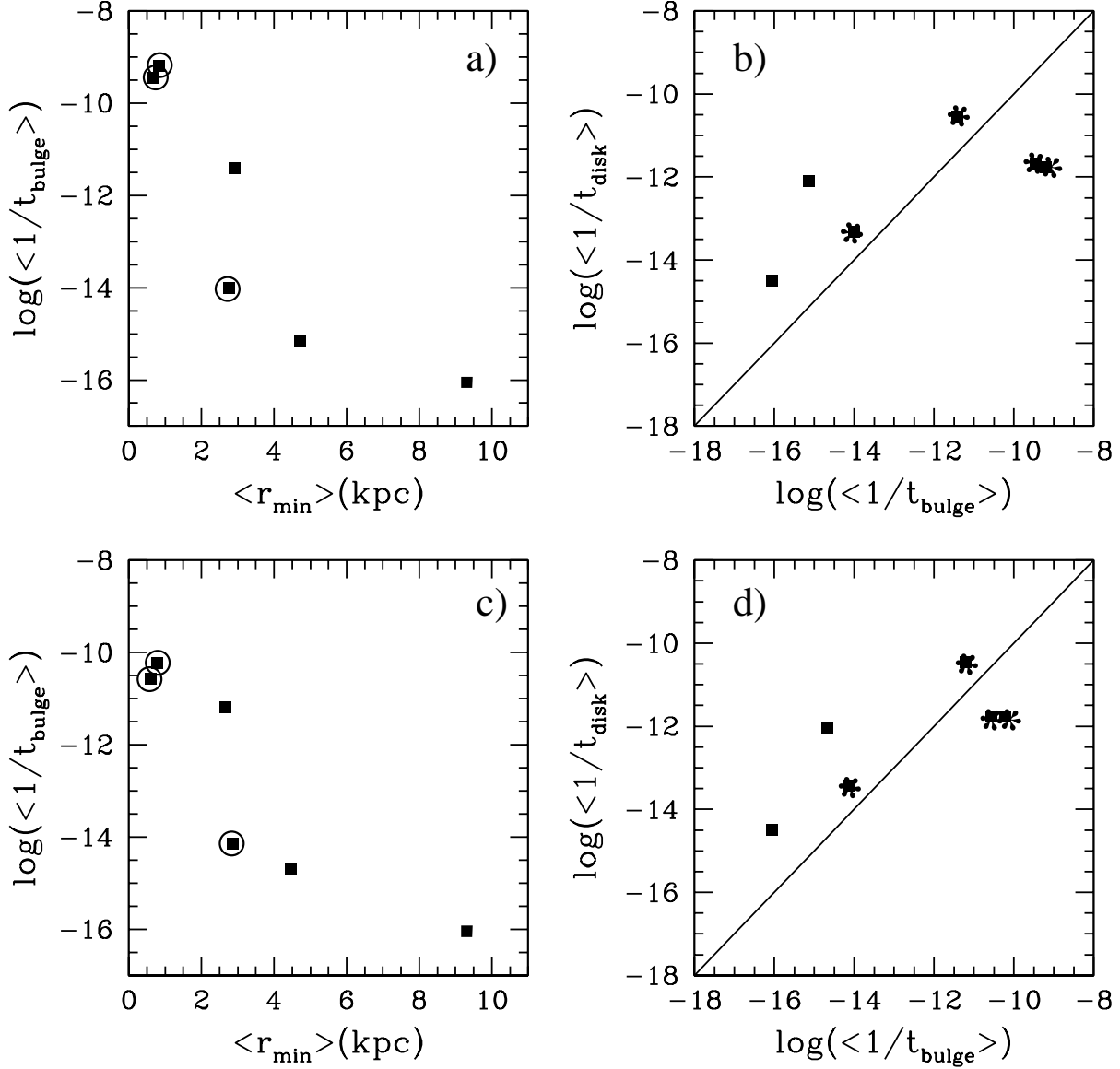


Fig. 11.— Destruction rates with the central orbits. We show the values of the total destruction rate due to the bulge as a function of  $\langle r_{\min} \rangle$ , the average minimum distance to the Galactic center, in (a) the axisymmetric, and (c) the non-axisymmetric potential. The marked squares correspond to clusters with  $\langle r_{\min} \rangle < 3$  kpc and orbital eccentricity  $e > 0.6$ . In (b) and (d) we give the comparison of the destruction rates due to the bulge and disk, in the axisymmetric and non-axisymmetric potentials, respectively. Marked squares correspond to clusters with  $\langle r_{\min} \rangle < 3$  kpc; the line of coincidence is plotted in both panels.